A multi-model approach for wooden furniture failure under mechanical load

Luc Chevalier, Florent Pled, Laura Winkler, François Wilquin, Eric Launay

Mechanics & Industry **23**, 28 (2022)

https://doi.org/10.1051/meca/2022025

Mechanics & Industry

Available online at:
www.mechanics-industry.org

REGULAR ARTICLE

OPEN ACCESS

A multi-model approach for wooden furniture failure under mechanical load

Luc Chevalier[1,*], Florent Pled[1], Laura Winkler[1], François Wilquin[2], and Eric Launay[2]

[1] Université Gustave Eiffel, Laboratoire Modélisation et Simulation Multi Echelle, MSME UMR 8208 CNRS, 77454 Marne-la-Vallée, France
[2] Institut technologique Forêt Cellulose Bois-Construction Ameublement, FCBA, 10 rue Galilée 77420 Champs-sur-Marne, France

Received: 31 January 2022 / Accepted: 18 September 2022

Abstract. Furniture failure generally appears at junctions between wooden parts. Failure prediction is a challenging problem considering the various technologies used for the assembly, the geometric dimensions of the wooden assembled parts and of the assembly components as well as the material properties of the wooden parts. Being able to provide a procedure for failure analysis is of great interest to the furniture industry. This paper proposes a multi-model approach in 3 steps: (i) a simplified global modeling of the whole structure (high loft bed) taking into account the specific geometry of each wooden part (beams or plates), (ii) a three-dimensional local numerical analysis of a through-bolt junction subjected to the mean critical load identified during a series of experimental compression tests to determine the local stresses in such a corner-type junction, and (iii) the application of an *ad hoc* failure criterion adapted to the anisotropic behavior of wood for failure prediction in through-bolt junctions.

Keywords: Wooden furniture / junction strength / multi-model / failure criteria

1 Introduction: industrial context and scientific goal

Loft bed and bunk bed furniture are widely produced for domestic use. Since furniture may be described as a mechanical structure submitted to various loadings [1], it can be classified into three groups depending on their structural design [2]:

- Frame-type structures constructed from beam-like elements of solid wood or wood-based materials, such as chipboard (or particleboard), Medium Density Fiberboard (MDF for short) or plywood.
- Structures constructed from plate-like elements of wood-based materials.
- Combined structures constituted of both beam- and plate-like elements.

The different components of such wooden structures are assembled with a variety of joining techniques. These techniques are either simple with only one or two fixing components or more complex. In this context, the FCBA Technological Institute (Forêt Cellulose Bois-construction Ameublement) and in particular the furniture division carries out normalized validation tests for furniture manufacturers. Its testing laboratory often declares the invalidity of furniture for which the normalized tests have led to unacceptable deterioration. During these mechanical strength tests, static or cyclic loads are applied on specific areas of the furniture. These tests are essential to ensure compliance with the furniture marketing standards, but they could be replaced by less expensive numerical simulations in a trial and error process that leads to the final design [3].

For safety reasons, CEN (the European Committee for Normalization) has issued a particular norm EN 747 [4] for this type of furniture which includes, in addition to dimensional control, validation tests for both static and dynamic loads. The strength and stiffness of wooden furniture are influenced by three main factors [5]: (i) the type of wood or wood-based materials from which furniture is made; (ii) the assembling technique used to join the elements, and (iii) the type of loading applied.

Wood-like materials exhibit a complex, heterogeneous and anisotropic behavior sensitive to hygrometric conditions and they are often modeled as classical orthotropic linear elastic materials to perform finite element simulations. Thanks to the numerous bibliographic references [6–16], the mean values for the spruce elastic properties are well known in the literature. Table 1 reports the mean

* e-mail: luc.chevalier@univ-eiffel.fr

Table 1. Transversely isotropic elastic properties for spruce.

Young modulus $E_r = E_t$	Young modulus E_ℓ	Shear modulus G_{rt}	Shear modulus $G_{r\ell} = G_{t\ell}$	Poisson ratio ν_{rt}	Poisson ratio $\nu_{r\ell} = \nu_{t\ell}$
500 MPa	11580 MPa	175 MPa	450 MPa	0.44	0.02

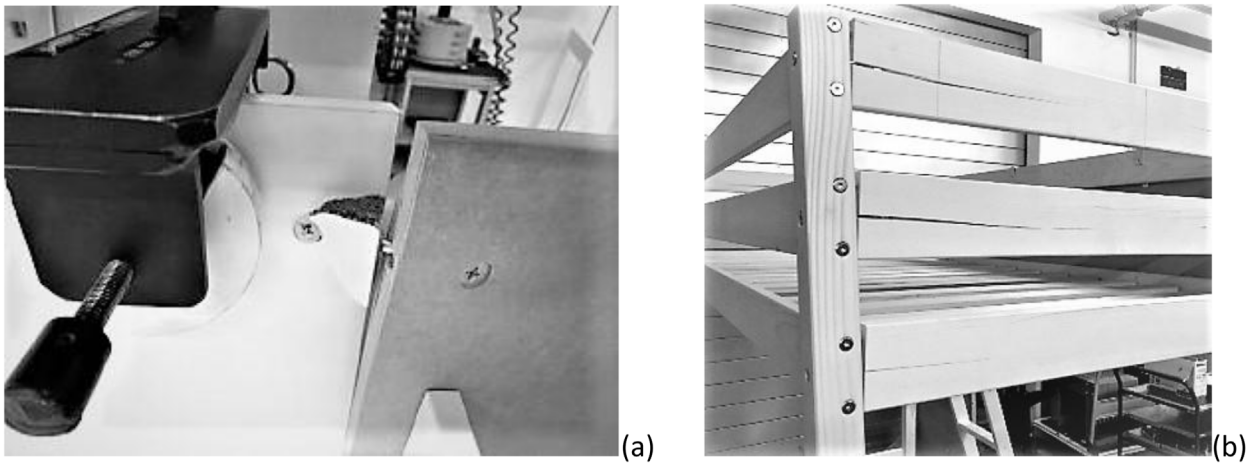

Fig. 1. Two main fracture modes for loft beds: (a) a transverse tearing fracture and (b) a typical cracking-induced failure.

values of transversely isotropic elastic properties for spruce wood taken from [17] (computed from the values given in [6–16]). The longitudinal Young modulus E_ℓ of spruce wood is greater than the radial and tangential Young moduli E_r and E_t in the cross section of the tree. E_r corresponds to the Young modulus in the radial direction of the expansion of the tree and represents more or less 4% of longitudinal Young modulus E_ℓ, while E_t corresponds to the Young modulus measured tangentially to the growth rings of wood and represents about 8% of E_ℓ. Even though the radial and tangential Young moduli E_r and E_t are not exactly equal (as well as Poisson ratios $\nu_{r\ell}$ and $\nu_{t\ell}$), we considered that spruce wood belongs to the class of transversely isotropic elastic materials so that the elastic properties are symmetrical with respect to the longitudinal axis corresponding to the wood fibers direction. We will further assume that the mean elastic behavior is transversely isotropic and homogeneous for our finite element simulations.

The mechanical strength properties are not so well known and in particular, in the radial and circumferential directions of the wood microstructure. These properties are however necessary to analyze the three-dimensional (3D) effects that appear in the junctions between furniture parts and are still the subject of ongoing research.

The method proposed in the present study is multi-model and is developed in three main steps. First, a statistical study conducted on 37 non-compliant experimental tests performed by FCBA has allowed to list and identify the most frequent failures. These generally appear at connections (or junctions) between furniture elements. The 37 aforementioned tests were carried out among a wide variety of furniture references with several types of connections, materials and defects. The experimental results highlight that the most frequent failure cases correspond to two fracture modes, that are the transverse tearing fracture of MDF plates (Fig. 1a) and the cracking-induced failure in spruce loft bed connections (Fig. 1b). The present study focuses on this last fracture mode.

The second step consists in developing a specific test in order to reproduce the fracture behavior and quantify the mechanical strength of spruce wood under complex loading. Here, the behavior of the specific assembly (through bolts, dowels, nuts, pins) used to fasten the main corner-type junctions in a wood loft bed frame under static or cyclic loads is modeled by connectors [18]. The through-bolt with a dowel-nut connection is of particular interest because of its mechanical strength and reliability [19], thus it is widely used to connect bed rails to bed posts although it can sometimes lead to failure, as shown in Figure 1. Thanks to the critical load value identified in the second step, the third and last step aims to evaluate an equivalent failure stress by comparing the experimental test result with the numerical stress distribution coming from a finite element simulation of this specific test. This critical failure stress will be necessary to build a failure criterion that can be used for all similar corner-type junctions even if the geometric dimensions are not exactly the same.

The remainder of the paper is structured as follows. Section 2 deals with the experimental aspects and presents the compression tests carried out on spruce samples including the geometric characteristics of the samples, the experimental protocol and the results obtained from these experimental tests, in particular the values of the measured critical load with the associated second-order statistics (mean value, standard deviation and dispersion).

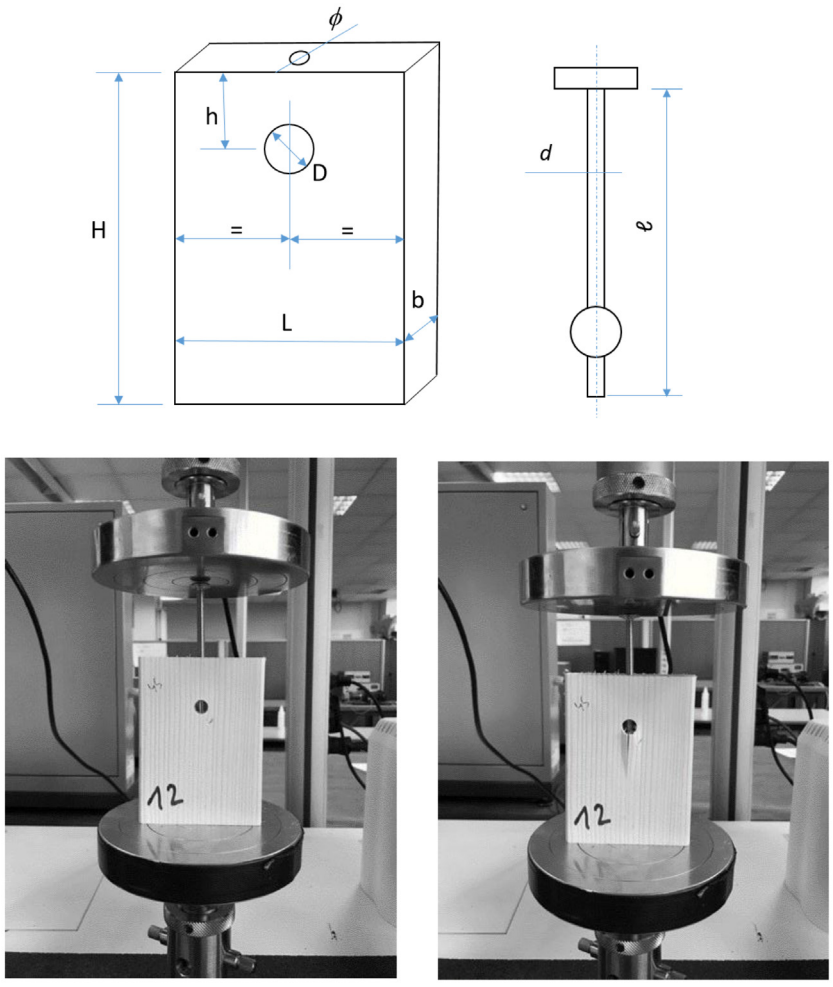

Fig. 2. (Top left) Geometry of the spruce specimens containing a horizontally centered circular through hole with diameter D and depth b (corresponding to the specimen depth), and a top circular non-through hole with diameter ϕ and a depth of 55 mm. (Top right) Geometry of the screw with length ℓ and diameter d. (Bottom) Example of compression test performed on sample #12.

This experimental test is assumed to be representative of the main failure mechanism occurring at junctions between furniture parts. It also presents meso-scale bending tests performed on corner-type junctions with one or two through-bolts corresponding to one-screw or two-screws assemblies. Finally, it presents a macro-scale normalized validation test conducted by FCBA on a high loft bed that failed due to multiple cracks occurring at junctions.

Section 3 deals with the modeling and numerical aspects. First, we present semi-analytical models of the bending tests carried out on corner-type junctions with one-screw and two-screws assemblies. The model prediction of corner strength (critical bending moment passing through the junction) for both connection types is compared to the experimental results obtained in Section 2. Finally, a finite element modeling of the complete high loft bed using the Timoshenko beam theory is proposed and the maximum bending moment occurring at junctions are compared to the critical bending moment obtained from the experimental bending tests on corner-type junctions in Section 2 in order to confirm if failure may occur or not for each connection type (with one or two screws).

Lastly, Section 4 discusses and presents the three-dimensional finite element simulation of the compression test to analyze the local stress distribution in the through-bolt junction. A failure criterion based on maximum principal stress normal to the wood fibers is finally proposed to quantify the mechanical strength and predict the failure of a through-bolt junction.

2 Experimental aspects: failure analysis in wooden products

2.1 Compression tests on wooden parts

In order to generate a representative stress field leading to cracking failure, compression tests are carried out on specimens made up of spruce wood using a through-bolt connection component consisting of a screw and a nut. Twenty rectangular parallelepiped samples cut from a spruce bed rail (or traverse) provided by the FCBA have been tested in this way. The geometric dimensions chosen for the test wood samples and standard carbon-steel based screws and nuts are shown in Figure 2 and given in Table 2.

Table 2. –Geometric dimensions of the samples, screw and nut.

Geometric dimensions	Values [mm]	Geometric dimensions	Values [mm]
Height H	120	Diameter ϕ of top non-through hole	7
Width L	90	Diameter D of center through hole	10
Depth b	20	Position h of center through hole	35
Length ℓ of the screw	100	Diameter d of the screw	5

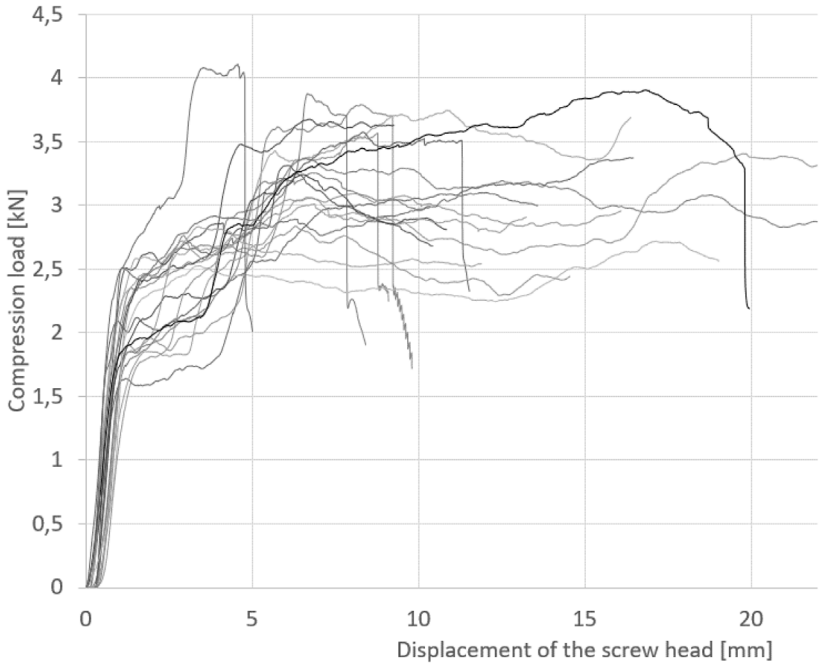

Fig. 3. Evolution of the measured load as a function of the imposed displacement of the screw head for each of the 20 compression tests.

The height H corresponds to the wood fibers direction. The compression machine on which the experimental tests were carried out is an INSTRON 3366 equipped with two circular compression plates and a computer software for the data acquisition of the applied load and corresponding displacement. For each sample of spruce wood, we use a screw of 100 mm long connected to a nut located in the center through hole of the specimen (Fig. 2, bottom). The screw is positioned at a depth of 50 mm inside the wood sample and 50 mm outside it. The specimen is simply placed at the center of the lower plate and the screw head is in contact with the upper plate which is vertically driven in displacement at a constant speed of 0.1 mm/s. The experimental test stops after the specimen breaks.

Two series of compression tests on spruce wood specimens that were cut from two different bed rails (having different orientations of wood fibers) were carried out for a total of 20 experimental tests. The evolution of the measured compression load versus the imposed displacement of the screw head is shown in Figure 3 for each test specimen. The deformation of the steel screw is not negligible compared to the deformation of the wood specimen under the nut but, in this study, we only focus on the critical load. The load-displacement curves in Figure 3 are not smooth in certain stages because of the complex microstructure of the wood material resulting in strongly anisotropic and heterogeneous mechanical properties. The fracture behavior of solid wood materials is usually considered as brittle provided the moisture content of the wood samples is sufficiently low (see [20] for an overview of the fracture properties of wood specimens).

Table 3. First- and second-order statistical data on the critical load obtained from the 20 compression tests.

First- and second-order statistics of critical load	
Mean value	2.25 kN
Standard deviation	0.30 kN
Dispersion	13.4%

The values of critical load, corresponding to the limit of the linear elastic behavior of the wood specimens, vary between 1.80 kN and 2.70 kN. One can also notice that the imposed displacement leading to complete failure highlights a strong dispersion. First- and second-order statistics have been calculated for the critical load. The mean value, the standard deviation and the dispersion (or coefficient of variation) of the critical load have been estimated from the 20 experimental data and are summarized in Table 3.

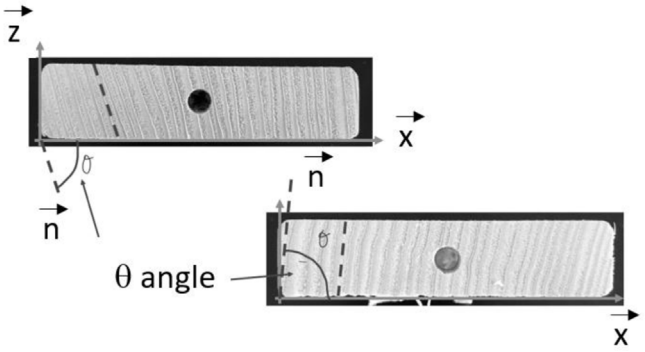

Fig. 4. Measure of the angle θ of the wood fibers orientation along the n-axis (circumferential direction represented in dashed line) with respect to the x-axis for two different wood specimens.

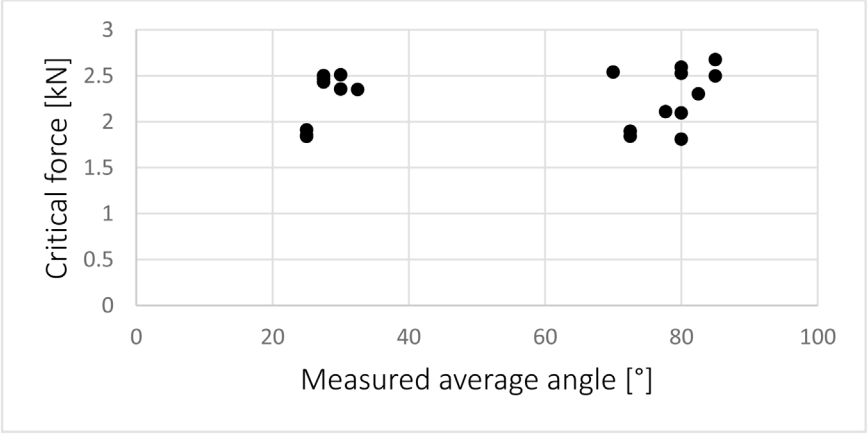

Fig. 5. Critical load as a function of the measured average angle of the wood fibers.

Considering the relatively important dispersion in the experimental data, we studied the possible influence of some wood characteristics on the critical loads such as the wood fibers orientation or the wood density. The angle of the wood fibers orientation in the transverse plane of isotropy, denoted $(\vec{x},\vec{z})$ in Figure 4, has been measured for all specimens. It corresponds to the angle between the x-axis and the n-axis in the circumferential direction of the wood fibers, as shown in Figure 4. It should be noted that the sign of this angle is not important here, and therefore only the absolute value is considered. The analysis of the influence of the wood fibers orientation on the critical load value from the 20 different samples shows that there is no correlation between the circumferential orientation and the critical load value as it can be seen in Figure 5. Indeed, the orientation of the wood fibers does not seem to have a major impact on the value of the measured critical load. Furthermore, the graph in Figure 5 simply highlights that the different orientations of the wood fibers can be separated into two groups, in that they are either between 25° and 35°, or between 70° and 85°. This is certainly due to the fact that the spruce wood specimens were cut from two different bed rails (or traverses), but in each group of specimens, one can see quite the same level of dispersion for the critical load.

2.2 Bending tests on corner-type junctions

In order to validate the choice of the simple compression test presented above, bending tests are performed on a loft bed corner assembly called hereinafter the corner-type junction or simply the corner. Different types of corners have already been studied in [17]. The corner-type junction considered here is composed of two spruce wood elements: a vertical part, the bedpost, and a horizontal part, the plank (or traverse). The experimental bending tests were carried out on a specific test bench designed to be adapted to the INSTRON compression machine (Figs. 6 and 7 for the one-screw and two-screws assemblies, respectively). Only 4 bending tests for the one-screw assembly and 5 bending tests for the two-screws assembly have been performed, so the calculation of mean values or standard deviations may be not really relevant here. The experimental bending tests were driven under displacement control at a constant speed of 0.05 mm/s for monitoring crack growth until (almost) complete failure.

In the one-screw assembly, the screw is positioned at the mid-height of the traverse, as shown in Figure 6. In the two-screws assembly, the two screws are both positioned at the same distance, $d = 34$ mm, from the mid-height of the traverse. The distance between the two screws is then equal

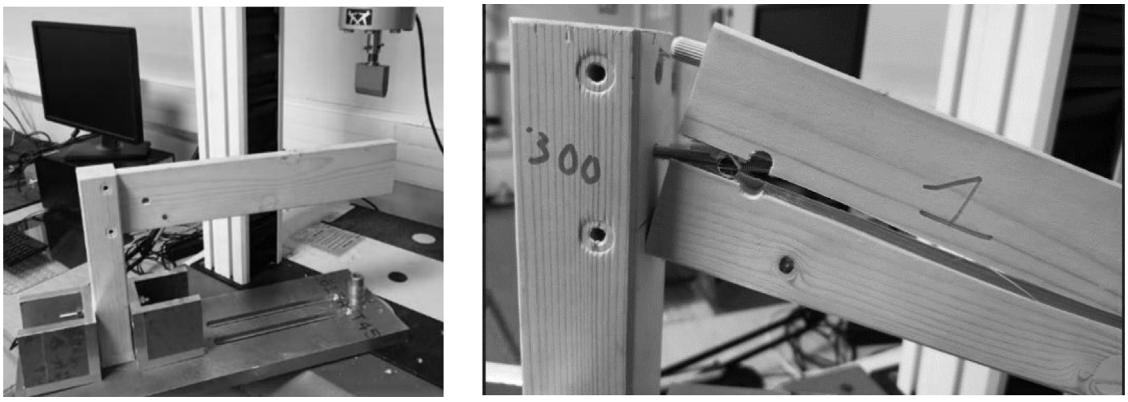

Fig. 6. One-screw assembly: (left) experimental test configuration and (right) resulting failure mode.

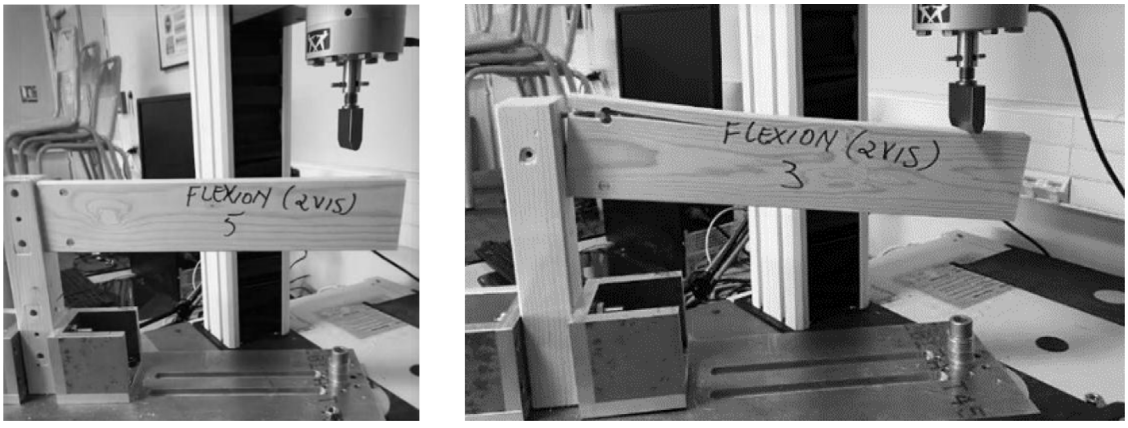

Fig. 7. Two-screws assembly: (left) experimental test configuration and (right) resulting failure mode.

to 68 mm. The wooden dowel seen on the picture is used to hold the traverse in position and does not contribute to the strength of the junction.

Figure 8 presents the results of the bending tests for the one-screw assembly. With the experimental device, we ensure that the bottom end of the vertical part (bedpost) is clamped to a rigid plate and that a vertical load is applied to the upper side of the horizontal part (plank) at a distance $d = 415$ mm from the vertical part (bedpost) of the corner-type junction. It is then possible to convert the vertical load F applied on the horizontal part (plank) into the bending moment M passing through the corner-type junction via the following simple relation: $MF \times L_t$ where L_t is the length of the wood horizontal part.

In Figure 8, one can identify the limit of the linear elastic behavior of the structure corresponding to the limit load in Table 4. A nonlinear behavior then occurs and all load-displacement curves show a maximal load value corresponding to the maximum load in Table 4. Both the limit loads and the maximum loads are indicated by downward vertical arrows respectively black and gray in Figure 8. To determine the values of limit load, we use the tangent method. A first straight line is drawn following the linear increase in load versus displacement and a second straight line is drawn following the smaller increase in load versus displacement in the nonlinear region. The limit load is then defined by the intersection of these two straight lines. The corresponding values of limit and maximum bending moments are also given in Table 4. It appears that the corner strength may vary from the average limit moment of 68 N.m to the average maximum moment of 113 N m.

The results of the bending tests carried out on the two-screws assembly are presented in Figure 9. One can notice that fracture occurs at a higher level of applied load that is almost twice as high as for the one-screw assembly.

Once again, we can evaluate the limit load and maximum load values for this test campaign. The results, including the limit and maximum bending moments passing through the corner-type junction, are summarized in Table 5. It is to be noted that we visually observed the crack initiation and crack growth, but we did not record the evolution of the crack trajectory during the experimental tests. It is difficult to localize accurately the crack initiation that occurs between points A and B (Fig. 9) that indicate respectively the limit load and the maximum load.

By using the two-screws assembly instead of the one-screw assembly, the maximum bending moment reaches an average value of 203 N m compared to 113 N m for the one-screw assembly (which corresponds to an increase of 1.8) and the limit bending moment reaches an average value of 135 N m compared to 68 N m for the one-screw assembly

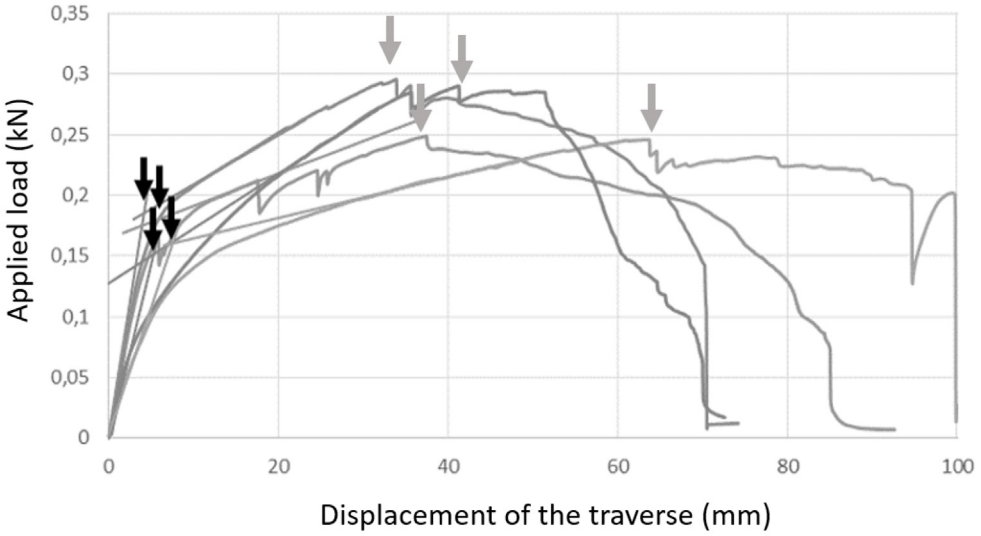

Fig. 8. One-screw assembly: evolution of the applied load as a function of the displacement. For each load-displacement curve, the intersection between the two tangential lines of the linear elastic behavior and of the first plastic zone defines the limit load (black arrow), while the discontinuity before complete failure defines the maximum load (gray arrow).

Table 4. One-screw assembly: summary table of limit and maximum load values.

Test #	1	2	3	4	Average
Maximum load [kN]	0.25	0.30	0.25	0.29	0.27
Maximum moment [N·m]	104	125	104	120	113
Limit load [kN]	0.17	0.18	0.16	0.15	0.17
Limit moment [N·m]	71	75	66	62	68

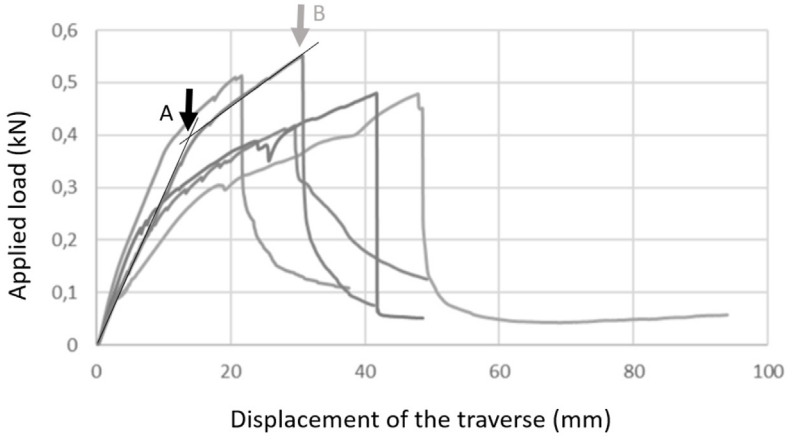

Fig. 9. Two-screws assembly: evolution of the applied load as a function of the displacement.

Table 5. Two-screws assembly: summary table of limit and maximum load values.

Test #	1	2	3	4	5	Average
Maximum load [kN]	0.49	0.51	0.42	0.48	0.55	0.49
Maximum moment [N·m]	203	212	174	199	228	203
Limit load [kN]	0.26	0.39	0.28	0.29	0.41	0.33
Limit moment [N·m]	108	162	116	120	170	135

Fig. 10. High loft bed after testing at FCBA: the three upper bed rails show horizontal crack propagation, while the fourth lower rail is completely broken and is laying on the side of the right bed post. All the geometric dimensions in the vertical direction (namely the heights H, H_1 and H_2) are measured from the floor.

Table 6. Geometric dimensions of the high loft bed.

Geometric dimensions	Values [mm]	Geometric dimensions	Values [mm]
Height H	1940	Height $2e$ of bed rail rectangular cross section	90
Length	1990	Thickness b of bed rail rectangular cross section	20
Width L	990	Height H_1 of bottom rail	620
Side length of bed post square cross section	50	Height H_2 of bed base	1530

(which corresponds to an increase of 2.0). Consequently, the use of two screws instead of one should be recommended in corner-type junctions that are likely to be subjected to a high level of bending moment.

2.3 Normalized tests on a high loft bed

The high loft bed (or mezzanine bed) chosen as a test case is made up of 4 vertical parts and several horizontal parts, respectively the posts (or legs) and the guard rails (or safety beams) that are shown in Figure 10. The different geometric dimensions of the loft bed are given in Table 6. On this test bed, a horizontal load F equal to 500 N is applied near the top junction as shown in Figure 10. This load of 500 N corresponds to an ultimate load value for the normalized validation tests under horizontal static loads performed on safety barriers at FCBA, according to the NF EN 747-1 § 4.1.4 and NF EN 747-2 § 5.4.2 standards for structural integrity [4]. More precisely, the horizontal force F is applied at a distance of 100 mm from the top corner-type junction and the normalized validation test on the safety barrier is driven under displacement control at a constant speed of 0.01 m/s until reaching the ultimate load value of 500 N. Several dozen validation tests have been performed at FCBA on high loft beds like the one presented in the present paper but with different geometric dimensions, under horizontal static loads. Only few of them led to cracking of the wooden horizontal traverses at

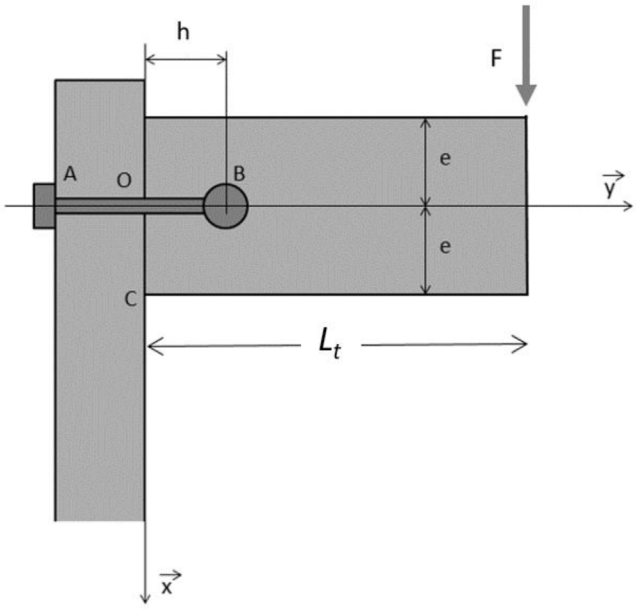

Fig. 11. One-screw assembly model for the through-bolt connection between two wooden parts of the high loft bed.

the junctions with the vertical bed posts, while the others passed the same mechanical test successfully. Only one experimental validation test was carried out on the high loft bed, with the specific geometric dimensions given in Table 6, that failed the mechanical test.

In Figure 10, one can observe that the high loft bed tested at FCBA did not pass the validation test successfully. First, all the three top rails (located around the elevated bed) are cracked: the cracks are deeper in the two upper guard rails than in the lower bed frame rail. Second, the bottom rail has come loose from the bed posts after cracking. The question then arises whether these experimental test results were predictable. The next section will present simple analytical models developed to derive the critical bending moment passing though the corner-type junction for both one-screw and two-screws assemblies directly from the mean critical load obtained from the compression tests in order to predict failure before carrying out the experimental validation test on the high loft bed.

3 Modeling: from compression tests to loft bed validation

In this section, two simple analytical models of the corner-type junction are proposed for both the one-screw and two-screws assemblies to represent the load distribution and to determine the relation between the bending moment passing through the junction and the tensile load in the screw(s).

3.1 Modeling the one-screw assembly

For the one-screw assembly case, Figure 11 illustrates the two-dimensional (2D) model used to analyze the bending test. Such 2D analytical model has already been presented in [21] in order to analyze the mechanical response of a corner-type junction (with one screw) in a loft bed under cyclic bending loading. Recall that the application of a load F at a distance d from the corner-type junction leads to a bending moment $M = L_t \times F$ passing through the (one-screw) assembly. All the geometric dimensions are identical to those of the real corner-type junctions (with one screw) used for the experimental bending tests presented in Section 2.2.

Because of the low rigidity of the vertical wooden part in the transverse direction, the screw head will penetrate the vertical wooden part (post) while the horizontal wooden part (plank or traverse) will sink into the vertical one over a height Δ near point C. We considered that the screw and nut are sufficiently rigid compared to the wood specimen. For all the experimental bending tests presented in Section 2.2, the screw remains straight after the test.

The value of distance Δ can be determined by considering that the normal load distribution is proportional to the depth of the local penetration of the plank into the post. To find this distance, the model proposed in Figure 12 is considered.

The plank (horizontal part) is submitted to a linear distribution of pressure $p(x)$ induced by the post (vertical part) over the distance Δ and which depends on the vertical position x measured from the middle of the horizontal part. This pressure field is due to the penetration $\delta_M(x)$ of the rigid horizontal part into the deformable vertical part at a point M belonging to the contact zone of length Δ. In parallel, the screw head penetrates into the vertical wooden part (post) at a depth δ and generates the rotation θ of the horizontal one (plank). A simple geometrical analysis then gives:

$$\delta_M(x) = \theta x - \delta. \tag{1}$$

The expression for distance Δ can be obtained by using the contact condition $\delta_M(x) > 0$ so that the contact zone extends from $x = \delta / \theta$ to $x = e$, which leads to:

$$\Delta = e - \frac{\delta}{\theta} = e - a \,\text{with:}\, a = \frac{\delta}{\theta}. \tag{2}$$

We assume the following linear relation $p(x) = K\,\delta_M(x)$ between pressure $p(x)$ and local penetration $\delta_M(x)$ and also the following linear relation $F_s/S = K\,\delta$ between the tensile load F_s in the screw and the horizontal displacement δ of the screw. S is the contact area under the screw head. Consequently, one can write the load and momentum balance equations for the horizontal wooden part as follows:

$$F_s = \iint_{\substack{contact \\ area}} p(x)dxdz = K(\theta e - \delta)b\frac{\Delta}{2} \,\text{and}\, M = \left(e - \frac{\Delta}{3}\right)F_s, \tag{3}$$

where b is the thickness of the horizontal part. Combining the above equation for F_s and the linear relation between F_s and δ leads to:

$$KS\delta = K(\theta e - \delta)b\frac{\Delta}{2} \Rightarrow \frac{b}{2S}(e-a)^2 - a = 0. \tag{4}$$

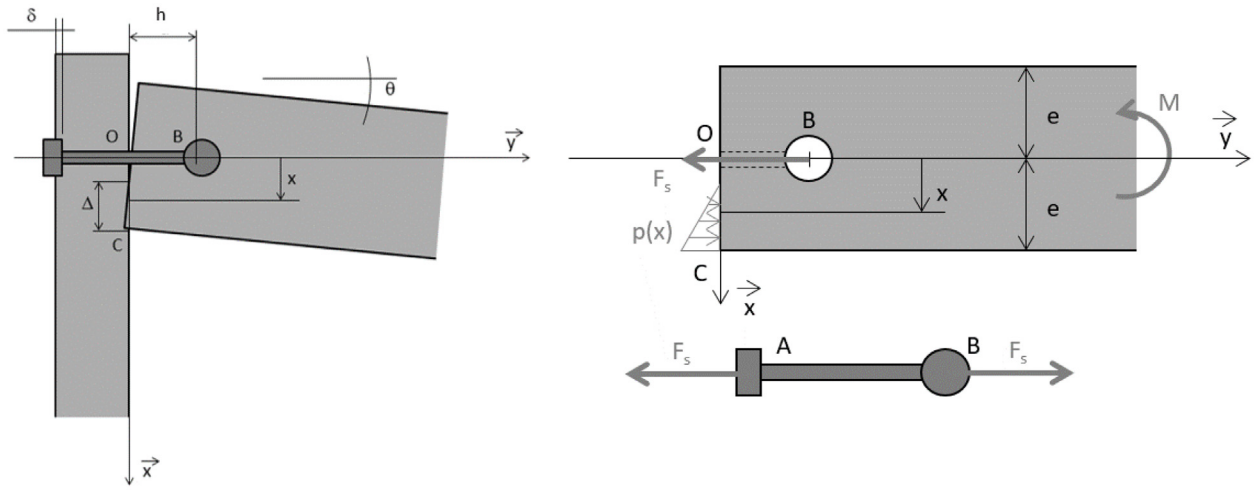

Fig. 12. One-screw assembly analysis: (left) rotation of the plank, horizontal displacement of the screw and local penetration of the plank into the post, (right) load distribution over the plank (top) and over the screw (bottom).

Solving this second-degree polynomial equation, we derive the following expression for length a:

$$a = e + \frac{S}{b}\left(1 \pm \sqrt{\left(1 + \frac{2eb}{S}\right)}\right). \tag{5}$$

Equation (5) with a minus sign gives a positive value for Δ. It should be noted that ratio a (or equivalently the length Δ of the contact zone) only depends on the geometric characteristics, but not on the applied force F. This results from the assumptions made on the linear relationship between the local pressure $p(x)$ and the local penetration $\delta_M(x)$ as well as the linear relationship between the tensile force F_s in the screw and the horizontal displacement δ of the screw. Both the rotation θ (with respect to the y-axis) of the traverse/plank and the penetration δ (horizontal displacement along the y-axis) of the screw head in the vertical post depend on the applied force F, but not the ratio a between penetration δ and rotation θ.

Using the numerical values $e = 45$ mm, $b = 20$ mm and $S = 85$ mm^2, we obtain $a = 29.2$ mm and the contact length $\Delta = 15.8$ mm. It is then possible to calculate the critical bending moment M_c when the tensile load F_s in the screw reaches the average critical value $F_c = 2.25$ kN obtained experimentally from the 20 compression tests: $M_c = (e\text{-}\Delta/3)\ F_c = 89$ N·m. This value lies in the interval between the average limit moment of 68 N· m and the average maximal moment of 113 N m obtained from the bending tests performed on the corner-type junction with one screw (see Sect. 2.2). Besides, the confidence interval of critical load F_c with a probability level of 0.99 can be estimated from the 20 experimental values of F_c and is equal to [1.81, 2.68] kN. The 99% confidence interval for the associated critical bending moment $M_c = (e\text{-}\Delta/3)\ F_c$ is then equal to [72, 106] N.m, which is very close to the interval [68, 113] N·m whose lower and upper bounds are the average limit and maximum bending moments, respectively. The experimental results of the bending tests are then in good agreements with the ones of the compression tests. Consequently, this confirms that the simple compression test proposed in Section 2.1 is representative of the cracking-induced failure mode in the corner-type junction for the one-screw assembly.

3.2 Modeling the two-screws assembly

In the case of a two screws assembly, a discussion is necessary to ensure that both screws are involved in the mechanical strength of the corner-type junction or that only one screw is involved. As we can see on Figure 13, the penetration of the horizontal wooden part (plank) into the vertical wooden part (post) near point C can lead either to the penetration of both screw heads into the vertical wooden part or to only the penetration of the top screw. In the first case, the horizontal displacements δ_b and δ_h of the two screws are both positive, whereas in the second case, only the value of δ_h is positive while that of δ_b is negative. As a result, if solving the problem leads to a negative value for δ_b, it means that the second case corresponds to the correct situation. We introduce the horizontal displacement δ at mid-height of the rigid horizontal wooden part which is defined, by symmetry of the problem, as:

$$\delta = \frac{\delta_h + \delta_b}{2}. \tag{6}$$

For numerical application, all the geometric dimensions are identical to those of the real corner-type junctions (with two screws) used for the experimental bending tests presented in Section 2.2.

As in the case of the one-screw assembly, we consider that the horizontal wooden part sinks into the vertical wooden part over a distance Δ near point C (Fig. 13). To find this distance, the model proposed in Figure 13 is considered. Note that equation (2) is still valid. First, let us assume that δ_b is positive so that both screws are involved in the junction strength. The load and

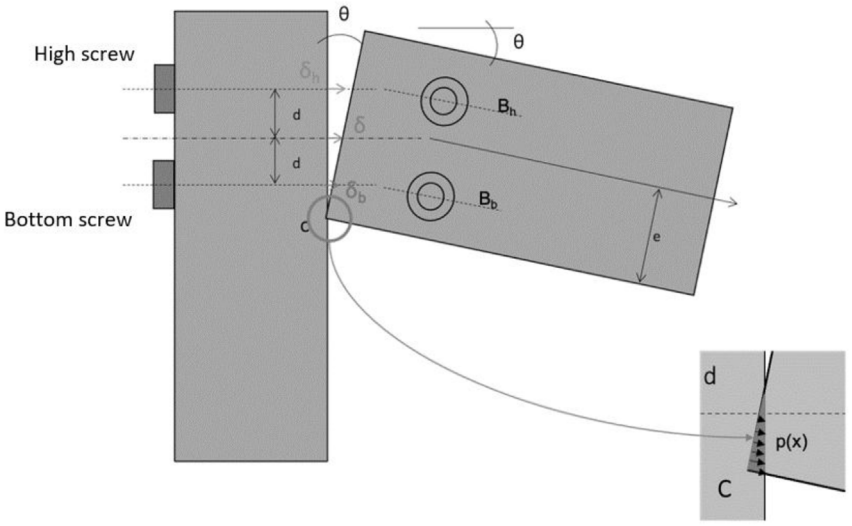

Fig. 13. Two-screws assembly model for the through-bolt connection between two wooden parts of the high loft bed.

momentum balance equations applied to the horizontal wooden part then lead to:

$$F_{sh} + F_{sb} = K(\theta e - \delta)b\frac{\Delta}{2} \text{ and } M = \left(e + d - \frac{\Delta}{3}\right)F_{sh} + \left(e - d - \frac{\Delta}{3}\right)F_{sb}, \quad (7)$$

where F_{sb} and F_{sh} are the tensile loads in the bottom and top screws, respectively. According to the previous equations, we have:

$$KS(\delta_h + \delta_b) = \frac{Kb}{2}\theta(e-a)^2. \quad (8a)$$

Then, introducing δ defined in equation (6) as the mean value of δ_b and δ_h, equation (8a) can be rewritten as follows:

$$\frac{b}{2S}(e-a)^2 - 2a = 0. \quad (8b)$$

Solving the second-degree polynomial equation (8b) leads to the following solutions for the length a:

$$a = e + \frac{2S}{b}\left(1 \pm \sqrt{1 + \frac{be}{2S}}\right) \quad (9)$$

and to the following values for the contact length $\Delta = e - a$:

$$\Delta = -\frac{2S}{b}\left(1 \pm \sqrt{1 + \frac{be}{2S}}\right). \quad (10)$$

Only one value of Δ is positive and with the numerical values $e = 45$ mm, $b = 20$ mm and S = 85 mm^2, we obtain the value $\Delta = 20.4$ mm for the contact length. The bottom screw is then inside the contact zone of length Δ. Consequently, there is no more contact between the bottom screw head and the vertical post, since the bottom screw is not loaded. Only the top screw is loaded, and therefore we can use the same model as for the one-screw assembly case but with a higher lever effect characterized by the vertical position $e + d$ of the top screw instead of the one e of the single screw as previously considered for the one-screw assembly.

By performing the calculations again and assuming only the top screw is loaded, we obtain the following new second-degree polynomial equation for the length a:

$$\frac{b}{2S}(e-a)^2 - (a+d) = 0 \quad (11)$$

whose solutions are given by:

$$a = e + \frac{S}{b}\left(1 \pm \sqrt{1 + \frac{2b}{S}(e+d)}\right) \quad (12)$$

and which leads to the following values for the contact length $\Delta = e - a$:

$$\Delta = -\frac{S}{b}\left(1 \pm \sqrt{1 + \frac{2b}{S}(e+d)}\right). \quad (13)$$

Finally, using the numerical values $e = 45$ mm, $b = 20$ mm, $d = 34$ mm and $S = 85$ mm^2, we obtain the value $\Delta = 22.0$ mm for the contact length. The penetration zone of the horizontal wooden part into the vertical wooden part is then 22 mm high. This value of 22 mm obtained for the two-screws assembly case is then slightly higher than the value of 15.8 mm obtained in the previous one-screw assembly case, but it is still compatible with the assumption that the bottom screw is not loaded. For the two-screws assembly, the critical bending moment M_c generated by the average critical load F_c can be evaluated as follows: $M_c = (e + d - \Delta/3)\ F_c = 162$ N·m. Similarly to the one-screw assembly, the confidence interval for a probability level 0.99 of the critical bending moment M_c can be

Table 7. Comparison between the bending test results and the predictions of the analytical model obtained from the critical load F_c of the compression test for the one-screw assembly (top) and the two-screws assembly (bottom).

One-screw assembly	Load [kN]	Corresponding bending moment	Moment [N·m]
Limit load F of bending test	0.17	$M = F$ x L_t	68
Maximum load F of bending test	0.27	$M = F$ x L_t	113
Critical load F_c of compression test	2.25 [1.81, 2.68]	$M_c = (e\text{-}\Delta/3)\ F_c$	89 [72, 106]
Two-screws assembly	Load [kN]	Corresponding bending moment	Moment [N.m]
Limit load F of bending test	0.33	$M = F$ x L_t	135
Maximum load F of bending test	0.49	$M = F$ x L_t	203
Critical load F_c of compression test	2.25 [1.81, 2.68]	$M_c = (e+d\text{-}\Delta/3)\ F_c$	162 [130, 192]

estimated using the 20 experimental values obtained from the compression tests and is equal to [130, 192] N ·m. It can then be compared to both the average limit and maximum bending moments measured during the bending tests performed on the corner-type junctions with two screws. The average limit bending moment is 135 N ·m, the average maximal bending moment is 203 N ·m, and the mean value of these two bending moments is 162 N ·m. All the results of the bending tests (for both the one-screw and two-screws assemblies) are summarized in Table 7 with the limit and maximum applied loads and the corresponding moment obtained via the simplified analytical model. These values are compared to the critical load and corresponding moment values obtained from the compression tests.

The average limit and maximum moments measured during the bending tests performed on the two corner-type junctions, namely the one-screw and two-screws assemblies, are then comparable to the confidence region for the critical moment predicted from the results of the compression tests on the spruce wood samples. Modeling the two-screws assembly case shows that the top screw takes almost all the bending moment and the lever arm is increased by the distance d compared to the one-screw assembly case. For the same critical load F_c applied to the (top) screw, the corresponding critical bending moment passing through the corner-type junction is higher for the two-screws assembly than for the one-screw assembly. Finally, the simple compression test proposed in Section 2.1 allows for the characterization of the cracking-induced failure mode occurring in corner-type junctions and thus can help to validate or not a loft bed design from a simple structural calculation.

3.3 Loft bed modeling

First, let us consider the two-dimensional problem of the front side of the high loft bed modeled as a planar portal frame with only one top beam and two posts (or columns) on pinned supports and submitted to a horizontal load F applied to the upper right corner, as shown in Figure 14. One can verify that the bending moment M captured by the corner-type junction is proportional to the height H of the structure, that is $M = X_B\ H$, where $X_B = F/2$ is the horizontal load at point B that is equal to half of the applied load F. It is worth pointing out that this expression does not depend on the width L of the structure and so this property cannot help to choose whether the screw(s) at the corner-type junctions should be placed along the length or the width of the loft bed.

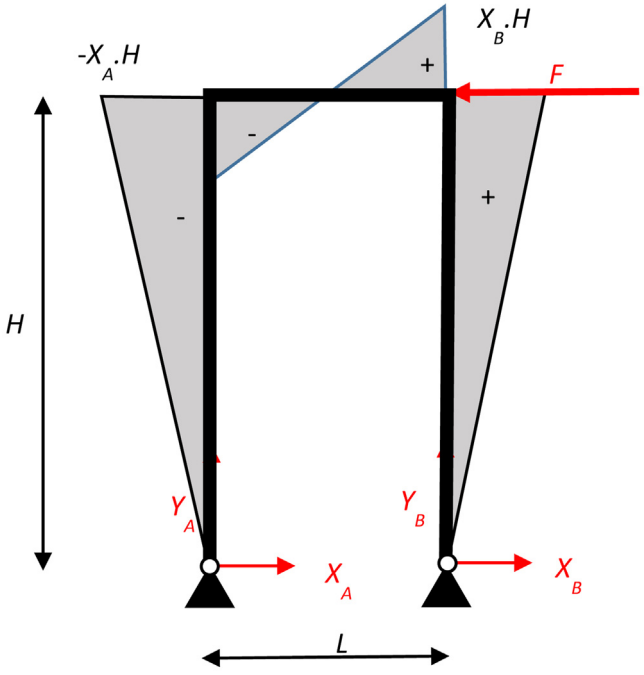

Fig. 14. Planar portal frame problem and bending moment distribution.

Consequently, the higher the loft bed is, the greater the bending moment in the junction is. For a loft bed of 1940 mm height subjected to a horizontal load $F = 500$ N, this would lead to a maximum bending moment $M = 485$ N ·m. This value is clearly not acceptable since the confidence interval corresponding to the probability level 0.99 for the critical

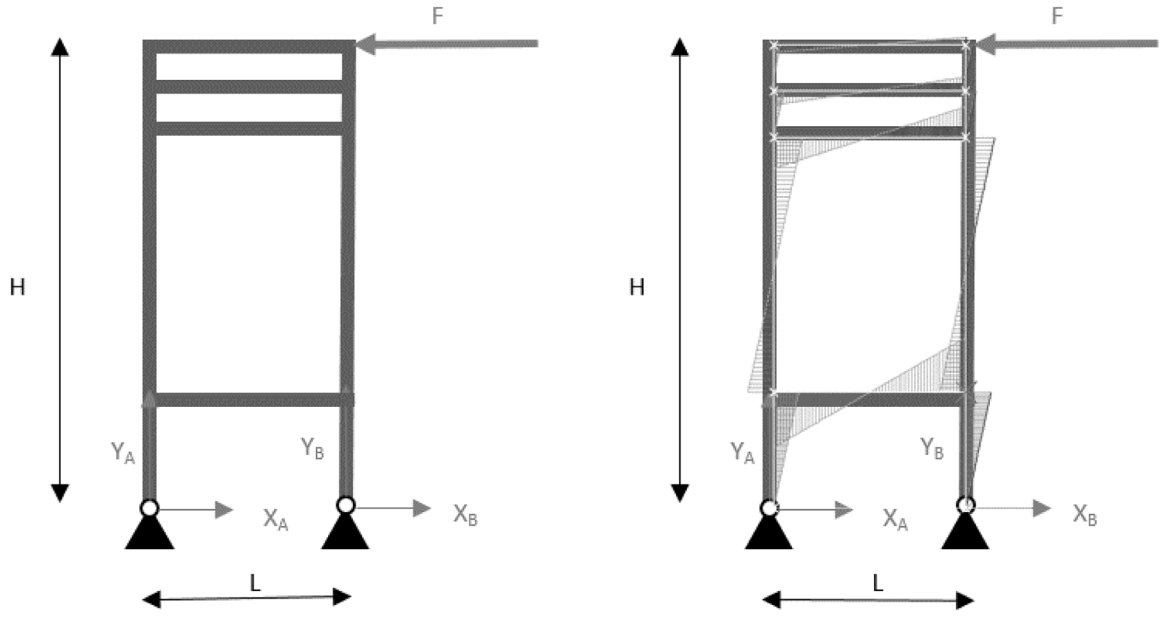

Fig. 15. Structure definition and bending moment diagram of the loft bed frame.

bending moment in the junction is equal to [72, 106] N·m for the one-screw assembly and [130, 192] N·m for the two-screws assembly. If one uses embedded boundary conditions at feet, the maximum bending moment is almost half the previous result with pinned feet on the floor. The conclusion remains the same: failure.

Using a finite element model with transversely isotropic Timoshenko beam elements, one can solve the more realistic two-dimensional problem of a high loft bed facade with three upper and one lower horizontal beams as in the real high loft bed. The geometry and boundary conditions are shown in Figure 15. The two vertical parts (posts or columns) are 1940 mm high with a square cross section of 50×50 mm^2. The four horizontal parts (beams) have a length of 990 mm and a rectangular cross section of 90×20 mm^2. Their vertical positions are respectively located at heights of 665, 1575, 1735 and 1895 mm. The horizontal load applied to the upper right corner is 500 N as in the validation tests carried out by the FCBA.

The analysis of the results shows that the reaction loads at points A and B are the same as for the simplified portal frame (with a single top beam). The bending moment in the vertical posts is maximum at the junctions with the lowest horizontal beam and reaches 155 N·m, and the bending moment in the horizontal beams is maximum in the lowest beam at the junctions with the vertical posts and reaches 256 N·m. Regardless of the assembly type considered (with one or two screws), this maximum bending moment of 256 N m is significantly higher than the extreme critical bending moment of 106 N· m (resp. 192 N· m) for the one-screw (resp. two-screws) assembly, and so the probability of failure is close to 100%. Consequently, the failure of the high loft bed occurs first at the bottom traverse, as observed experimentally (Fig. 10). After the lowest horizontal beam breaks, there is a load transfer, and the bending moment increases in the three upper horizontal beams until cracking occurs.

Considering the complete high loft bed and the fact that the external load is not applied exactly to the top corner-type junction, one can modulate this conclusion. The complete high loft bed is modeled as an assembly of beam elements with a bed base containing 14 slats (Fig. 16, top). The four vertical bed posts are clamped at their respective lower ends, while an outward horizontal load $F = 500$ N is applied at a distance of about 100 mm from the upper corner-type junction. The numerical simulation results, coming from an in-house research finite element code developed in Matlab, are shown in Figure 16, bottom.

The maximum bending moment in the two front vertical posts of the high loft bed is obtained at the junction with the bed base and reaches the value $M = 109$ N·m, while the maximum bending moment in the lowest front horizontal beam (bottom traverse) occurs at the junctions with the bed posts and reaches a higher value $M_{max} = 158$ N·m. Note that these values are significantly lower than the one predicted by the previous two-dimensional (planar) model of the high loft bed façade. This is probably due to the global torsion of the loft bed structure and the consideration of the slats that tend to reduce the bending effects.

Considering the confidence region of the critical bending moment M_c (with a probability level of 0.99) estimated in Section 3.1 (resp. Sect. 3.2) for the one-screw (resp. two-screws) assembly, one can predict that the failure of the corner-type junction is very likely to occur for a single-screw assembly, while the corner-type junction may resist with a two-screws assembly.

This last study illustrates that it is possible to give a good prediction of the failure risk for a high loft bed without resorting to costly experimental validation tests in the FCBA laboratories. However, the practical use of this prediction is limited to some particular conditions: (i) the high loft bed must be made of spruce (the wood material for which the compression tests were carried out in Sect. 2.1); (ii) the screws and nuts used during the bending tests

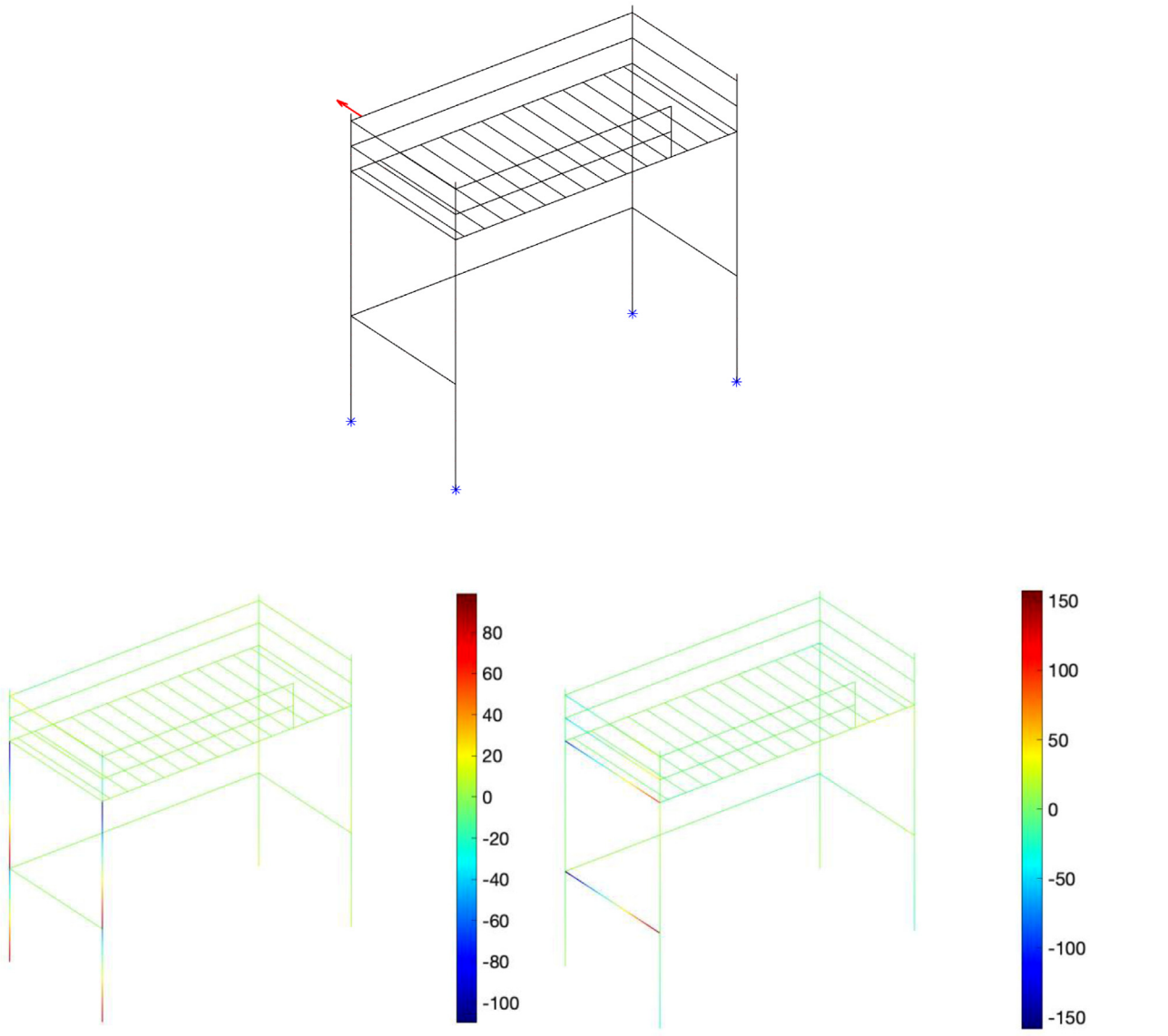

Fig. 16. High loft bed modeled by a beam assembly (top), bending moment in the vertical bed posts (bottom left), and bending moment in the horizontal beams (bottom right), with values given in [N· m].

performed on the corner-type junctions in Section 2.2 must be the same as those of the high loft bed whose strength is to be determined. Nevertheless, thanks to the simple analytical models of the corner-type junction with one-screw and two-screws assemblies proposed in Sections 3.1 and 3.2, it is possible to vary the height of the traverse cross section. In the next section, we discuss a failure criterion involving only the wood material properties (and not the geometric dimensions) in order to circumvent or at least mitigate these limitations.

4 Discussion: failure criterion for through-bolt junctions

The experimental compressive tests allow for identifying a global critical load F_c that depends on the specimen dimensions, in particular the nut diameter and the wooden part thickness. In order to extend and generalize the experimental results to other geometric dimensions, it would be interesting to build a fracture criterion that depends on the wood material properties but not on the geometric properties of the test specimen. The finite element modeling and numerical simulation of the compression test will allow for making the correspondence between the critical load F_c and the local stresses.

4.1 Numerical simulation of the compression test

The three-dimensional numerical simulation of the compression test is carried out using Abaqus CAE software (Fig. 17). The wooden part is modeled as a rectangular parallelepipedal solid made up of an orthotropic linear elastic material (spruce wood). The screw and nut assembly forming the through-bolt is considered as a single solid made up of an isotropic elastic material (steel).

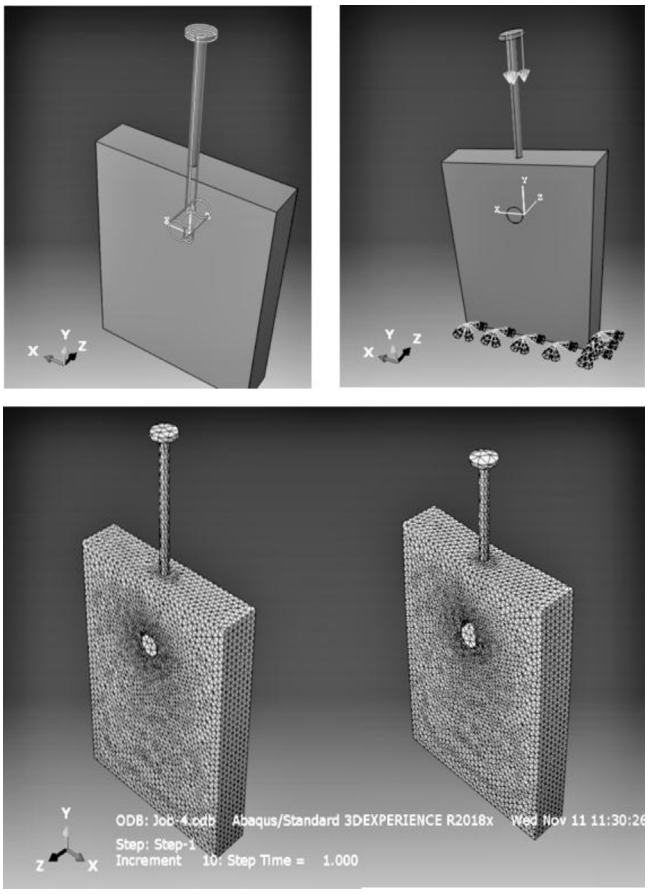

Fig. 17. (Top) Assembly and boundary conditions, (Bottom) mesh and deformed structure.

Frictional contact conditions are enforced at the interface between wood and steel parts with a specific coefficient of friction μ. From [22], the mean value of friction coefficient μ is around 0.15 for a smooth surface and about 0.45 for a rough surface, so that choosing $\mu = 0.3$ is a good compromise. Note that this value does not seem to have a strong influence on the numerical results, since we did not see any noticeable difference in the finite element stress distribution for different values of friction coefficient μ varying from 0.1 to 0.5.

As regards the other boundary conditions, the bottom end surface of the wooden part is clamped, and the assembly is subjected to a surface load uniformly distributed over the screw head (for an equivalent load of 2.25 kN).

In the model shown in Figure 17, the y axis denotes the direction of the wood fibers and also the direction of the applied loading. The surface load imposed on the screw head corresponds to a pressure of 20 MPa. The screw is simply modeled as a cylinder with no filet and a diameter 3 times smaller than that of the screw head. The numerical results show that the maximum normal stress in the screw reaches $\sigma_{yy} = 180$ MPa which is a relatively high value for a steel screw. Recall that the experimental tests have led to an average critical load equal to 2.25 kN.

For this compression load, the local stresses in the x-y plane, around the hole (nut housing) at the bottom of which the cracking failure initiates, are shown in Figure 18 and summarized hereinafter:

- Tensile stress $\sigma_{xx} = 1.7$ MPa at the bottom of the hole;
- Compressive stress $\sigma_{yy} = -15.3$ MPa at the bottom of the hole;
- Tensile stress $\sigma_{yy} = 12$ MPa at the left and right edges of the hole;
- Shear stress $\sigma_{xy} = -1.5$ MPa near the hole in the plane inclined at 45 degrees (with respect to the z axis) and passing through the axis of revolution of the hole. Shear stress is zero at the bottom of the hole.

The normal stress field σ_{yy} corresponds to the stress field in the wood fibers (longitudinal) direction. It takes higher values than the normal stress field σ_{xx} in the transverse direction, but the wood strength is also higher in the longitudinal direction (along the y axis) than in the transverse directions (along the x and z axes). In the region located at the bottom of the hole (under the nut housing), σ_{yy} is a compression stress field, while σ_{xx} is a tension stress field, and since the tensile strength is very low in the transverse directions of wood material, this tensile stress will generate a crack emerging from the bottom of the hole and propagating downwards (consistently with that

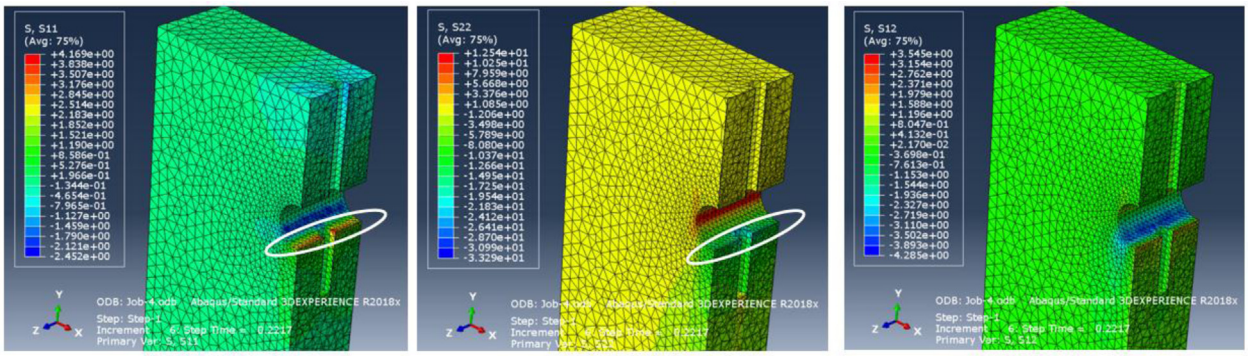

Fig. 18. Stresses σ_{xx}, σ_{yy} and σ_{xy} in the wooden part of the assembly.

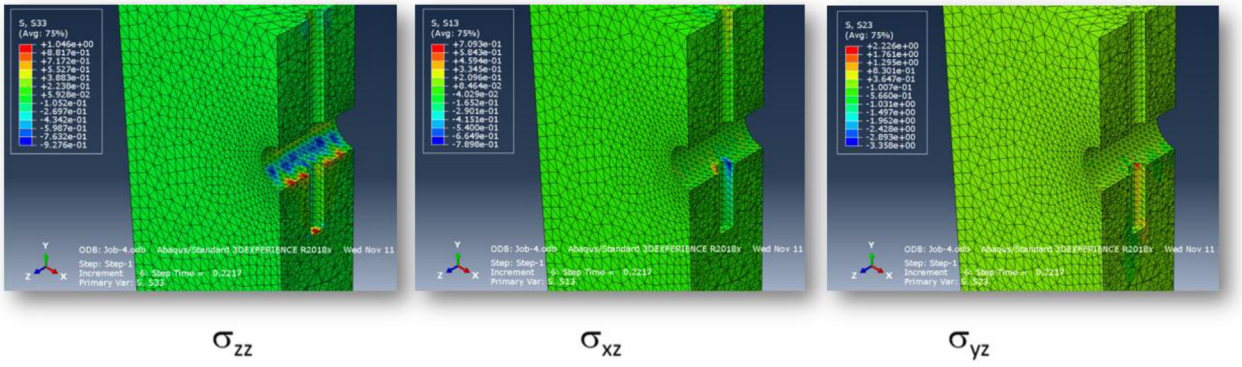

Fig. 19. Stresses σ_{zz}, σ_{xz} and σ_{yz} in the wooden part of the assembly.

observed in Figure 2, right during the experimental compression tests), thus leading to cracking-induced fracture.

Figure 19 shows the local stresses in the z direction whose maximum values around the hole are given hereinafter:

– Tensile stress $\sigma_{zz} = 0.69$ MPa;
– Shear stress $\sigma_{xz} = 0.0074$ MPa;
– Shear stress $\sigma_{yz} = 0.063$ MPa.

Except the tensile stress σ_{zz}, the shear stresses σ_{xz} and σ_{yz} are negligible with respect to the local stresses in the x-y plane. The three-dimensional problem can then be considered as quasi-planar in the x-y plane.

4.2 Failure criterion for the through-bolt junction

Following these results, one can propose a fracture criterion based on the transverse tensile stress σ_{xx} with a mean value for the critical failure stress $\sigma_c = 1.7$ MPa that corresponds to the mean critical load $F_c = 2.25$ kN identified from the compression tests. In the general case, the Rankine like failure criterion (maximum principal stress) may be expressed as:

$$\sup_{i=1,2}(\sigma_i) \leq \frac{\sigma_c}{s}, \tag{14}$$

where σ_i are the principal stresses (with $i = 1, 2$) in the normal plane to fibers and s is a security factor that may be considered by the furniture producer for safety reasons. A typical value for the safety factor s used in the furniture industry is 1.2. In the particular case considered in this work, the maximum principal stress corresponds to the transverse tensile stress σ_{xx} localized under the nut housing. From the dispersion observed on critical load F_c, the standard deviation for the failure stress σ_c can be estimated and is equal to 0.22 MPa. Figure 20 shows the evolutions of the probability density function (pdf) and cumulative distribution function (cdf) of an approximate normal distribution for failure stress σ_c which can be used to evaluate the probability of failure. For example, if the local tensile stress σ_{xx} is equal to 2 MPa, then the probability of failure is approximately 90%, but if the stress only reaches 1.5 MPa, then this probability falls to only about 20%.

To complete this criterion, one can study the influence of the junction geometry on the critical stress by performing numerical simulations of the through-bolt junction with different geometric dimensions. On the one hand, the influence of some geometric parameters, such as the thickness of the wooden part for example, is quite obvious, since if the traverse (wooden part) has a wider thickness, then the applied load will be distributed on a larger surface and consequently the resulting local stresses

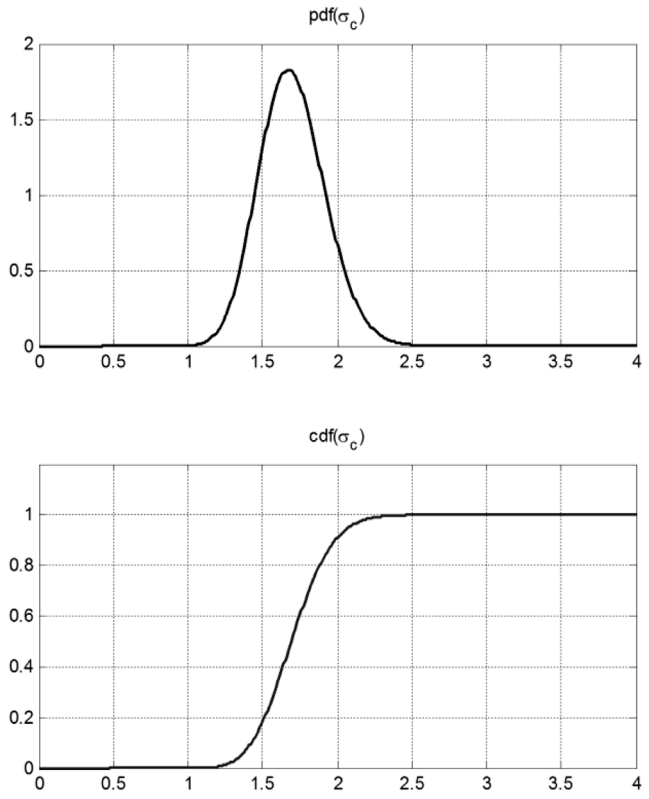

Fig. 20. Probability density function (top) and cumulative distribution function (bottom) for failure stress σ_c expressed in [MPa].

will reduce proportionally. On the other hand, the impact of some other geometric parameters, such as the nut diameter for example, is more difficult to anticipate because of the local curvature and the effect of friction that would require additional numerical simulations to conclude. Thanks to these simulations, one could then evaluate the new critical load without managing new series of experimental tests. Finally, it should be noted that other geometric parameters, such as the height of the transverse cross section, the position of the screw or the diameter of the screw head for example, could also be modified in the analytical model of the corner-type junction proposed in Section 3.1 in order to analyze their influence on the limit bending moment.

5 Conclusion

A multi-model approach to characterize the mechanical strength and predict the cracking-induced failure of spruce wooden furniture subjected to mechanical loads has been presented in this paper. A series of compression tests on standardized spruce samples cut from a high loft bed has been carried out to obtain experimental data corresponding to the measured critical load values and compute the associated first- and second-order statistics (mean value, standard deviation and dispersion). Complementary bending tests on corner-type junctions consisting of one-screw and two-screws assemblies have been performed to derive the critical bending moment passing through the junction for both connection types (one-screw and two-screws assemblies). Simple analytical models of the corner-type junction have also been proposed for each connection type. From the experimental test results and the analytical models of the corner-type junction, it can be concluded that the compression test is representative of the cracking-induced failure mechanism occurring in the corner-type junctions for both one-screw and two-screws assemblies. Indeed, the results show that the range of critical bending moment values calculated from the critical load values measured during the compression tests on spruce wood samples is close to the range defined by the average limit and maximum bending moments measured during the bending tests performed on the corner-type junctions for both one-screw and two-screws assembly cases.

For validation purposes, the complete high loft bed from which the spruce wood samples were cut for the compression tests had been previously tested and submitted to a static horizontal load leading to complete failure due to multiple cracks occurring at corner-type junctions. Different finite element models with beam elements have been constructed for simulating the mechanical response of the high loft bed façade in two dimensions and that of the complete high loft bed in three dimensions. The numerical results show that failure is very likely to occur for the most loaded corner-type junction with a single-screw assembly as experimentally observed in the real validation test. Lastly, a three-dimensional finite element model of the compression test is constructed to compute the local stress field in the through-bolt junction. A failure criterion based on maximum principal stress normal to the wood fibers is finally applied to characterize the mechanical strength and predict the failure of a through-bolt junction.

In summary, the proposed multi-model approach consists in calculating the generalized stresses (stress resultants) passing through the connections in wooden furniture at the structure scale using a beam finite element code. From an analytical modeling of the connection, one can deduce the resulting local load in the connecting elements. This load is then compared to the critical mechanical strength identified during a simple experimental test characteristic of the degradation (failure) mode of the connection. From a local 3D finite element simulation of this specific test, the local stresses are finally evaluated and allows the extension of the approach to different geometric features of the connection.

References

[1] A. Kasal, Determination of the strength of various sofa frames with finite element analysis, Gazi Univ. J. Sci. **19**, 191–203 (2006)
[2] H.I. Demirci, The experimental and finite element analysis of diagonal tensile tests conducted on frame-type constructed corner joints, Technology **14**, 11–21 (2011)
[3] H. Makhlouf, L. Chevalier, E. Favier, E. Launay, A stochastic approach for the evaluation of the reliability of wood furniture in an industrial context: managing virtual standardization tests, Mech. Ind. 17 (2016)

[4] European Committee for Standardization CEN, EN 747, Furniture – Bunk beds and high beds for domestic use – Part 2: test methods, https://standards.globalspec.com/std/9934832/en-747-2,2012-present.
[5] T. Nicholls, R. Crisan, Study of the stress strain state in corner joints and box-type furniture using Finite Element Analysis (FEA), Eur. J. Wood Wood Prod. **60**, 66–71 (2002)
[6] J.E. Winandy, Wood properties, Encyclop. Agric. Sci. **4**, 549–561 (1994)
[7] J. Bodig, B. Jayne, Mechanics of Wood and Wood Composites (Krieger Publishing Company, 1993)
[8] D. Guitard, Mécanique du matériau bois et composites, Edition Cépaduès (1987)
[9] J. Campredon, Contribution à l'étude des propriétés élastiques des bois, Annales de l'école nationale des eaux et forêts et de la station de recherches et expériences, **3**, 251–288 (1935)
[10] P. Niemz, D. Caduff, Research into determination of the Poisson ratio of spruce wood, Holz Roh Werkst **66**, 1–4 (2008)
[11] F.H. Neuhaus, Elastizitätszahlen von Fichtenholz in Abhängigkeit von der Holzfeuchtigkeit, 1981 edn. (Institut für Konstruktiven Ingenieurbau, Ruhr University, 1981)
[12] E. Kahle, J. Woodhouse, The influence of cell geometry on elasticity of softwood, J. Mater. Sci. **29**, 1250–1259 (1994)
[13] H. Carrington, The elastic constants of spruce, Philos. Mag. **45**, 1055–1057 (1923)
[14] D. Keunecke, W. Sonderegger, K. Pereteanu, T. Lüthi, P. Niemz, Determination of Young's and shear moduli of common yew and Norway spruce by means of ultrasonic waves, Wood Sci. Technol. **41**, 309–327 (2007)
[15] Forest Products Laboratory, Wood Handbook: Wood as an Engineering Material (USDA, Forest Service, Forest Products Laboratory, 1999)
[16] J. Charles, Wood properties, Encyclop. Agricult. Sci. **4**, 549–561 (1994)
[17] L. Chevalier, H. Makhlouf, B. Jacquet-Faucillon, E. Launay, Modeling the influence of connecting elements in wood products behavior: a numerical multi-scale approach, Mech. Ind. **19**, 301 (2018)
[18] Y.Z. Erdil, J. Zhang, C.A. Eckelman, Withdrawal and bending strength of dowel-nuts in plywood and oriented strand board, Forest Prod. J. **53**, 54–57 (2003)
[19] C.A. Eckelman, Holding strength of through bolt with dowel nut connections, Forest Products J. **39**, 41–48 (1989)
[20] M.P.C. Conrad, G.D. Smith, G. Fernlund, Fracture of solid wood: a review of structure and properties at different length scales, Wood Fiber Sci. **35**, 570–584 (2003)
[21] L. Chevalier, F. Pled, F. Zambou, E. Launay, Cyclic virtual test on wood furniture by Monte Carlo simulation: from compression behavior to connection modeling, Mech. Ind. **20**, 606 (2019)
[22] W.M. McKenzie, H. Karpovich, The frictional behaviour of wood, Wood Sci. Technol. **2**, 139–152 (1968)

Cite this article as: Luc Chevalier, Florent Pled, Laura Winkler, François Wilquin, Eric Launay, A multi-model approach for wooden furniture failure under mechanical load, Mechanics & Industry **23**, 28 (2022)